ARTICLE IN PRESS

Available online at www.sciencedirect.com

SCIENCE DIRECT®

ELSEVIER

International Journal of Impact Engineering ▮ (▮▮▮▮) ▮▮▮–▮▮▮

INTERNATIONAL JOURNAL OF IMPACT ENGINEERING

www.elsevier.com/locate/ijimpeng

Modeling prestressed ceramic and its effect on ballistic performance

Timothy J. Holmquist*, Gordon R. Johnson

Army High Performance Computing Research Center/Network Computing Services, Inc., P.O. Box 581459, Minneapolis, MN 55458-1459, USA

Received 29 May 2003; received in revised form 10 November 2003; accepted 12 November 2003

Abstract

This article presents computed results for the responses of ceramic targets, with and without prestress, subjected to projectile impact. Also presented is a computational technique to include prestress. Thin and thick ceramic target configurations are used to understand the effect prestressing has on ballistic performance. For both targets two prestress levels (small and large), and two prestress states (radial and hydrostatic) are investigated. The small prestress is similar in magnitude to values obtained experimentally and the large prestress is approximately the maximum prestress the confinement can produce (determined computationally). The targets are subjected to projectile impact and the resulting ballistic responses are evaluated. In all cases prestressing the ceramic enhanced the ballistic performance, although the effect of the different prestress conditions on the ballistic response was not always obvious.

Keywords: Ceramic; Prestress; Damage; Penetration

1. Introduction

Ceramic materials have been considered for armor applications for over 30 years [1]. Generally, these materials are very strong in compression and weak in tension. They are also very brittle, but can have significant strength after failure when under compression. Both the intact and failed materials generally are pressure dependent where the strength increases as the confining pressure increases. The amount of inelastic (plastic) strain the material can withstand before failure is also pressure dependent, where the plastic strain to failure increases as the pressure increases. Effective armor design attempts to take advantage of the pressure dependency ceramics exhibit. It is well documented that adding confinement to ceramics increases its ballistic performance [2]. More

*Corresponding author. Tel.: +1-612-337-3561; fax: +1-612-337-3400.
E-mail address: tjholm@networkcs.com (T.J. Holmquist).

0734-743X/$ - see front matter © 2003 Elsevier Ltd. All rights reserved.
doi:10.1016/j.ijimpeng.2003.11.002

recently, using the confinement to "prestress" the ceramic is being considered for additional ballistic improvement [3,4]. By prestressing ceramic in compression, both the strength and ductility are increased. The prestress also protects the ceramic from premature failure in tension.

Recently, the authors developed a computational technique to include prestress for confined ceramic targets [5]. The authors used the technique to produce a small prestress (similar to experimental levels) in a thin and thick target. This earlier work showed that even a small prestress improved the target's ballistic performance. It also indicated that the type of prestress (radial or hydrostatic) could affect the ballistic response. The work reported herein extends the original work to much larger prestress conditions. Here the prestress condition is increased to the limit the target configuration will allow. The ballistic performance (dwell, penetration and perforation) is used to evaluate the prestressed targets.

2. Ceramic prestress

Fig. 1 shows computed results for a prestressed axisymmetric target. The target consists of AD99.5 alumina ceramic surrounded by titanium confinement. This configuration was chosen because there are experimental data available [3]. Meyer et al. used a hot isostatic press (HIP) process to prestress the target. Neutron diffraction was used to measure the axial, radial, and

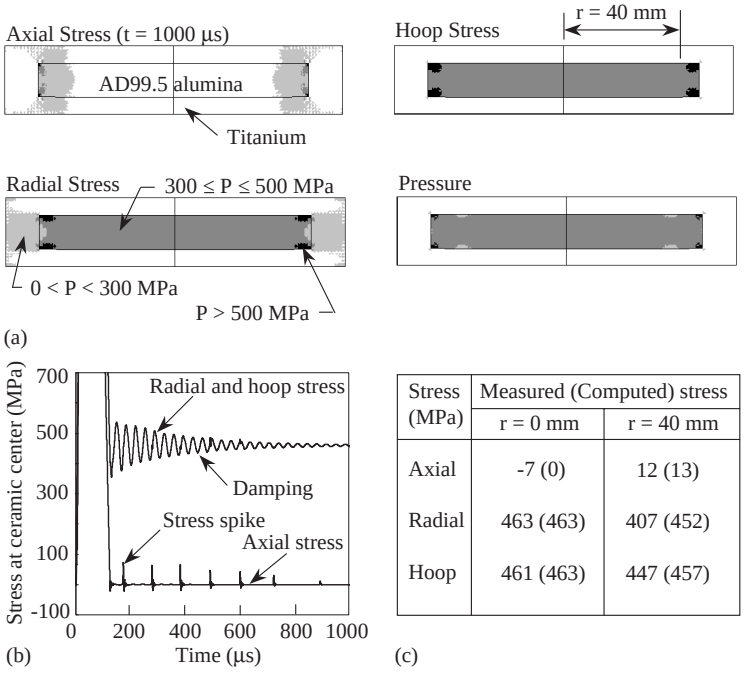

Stress (MPa)	Measured (Computed) stress	
	r = 0 mm	r = 40 mm
Axial	-7 (0)	12 (13)
Radial	463 (463)	407 (452)
Hoop	461 (463)	447 (457)

Fig. 1. Computed results for a thin, prestressed ceramic target. (a) Final ($t = 1000\,\mu s$) computed axial, radial, hoop and pressure stress contours in the target (compression is positive). (b) Computed axial, radial and hoop stress histories measured at the center of the ceramic. (c) Comparison between the computed and measured stresses at a radius of 0 and 40 mm in the ceramic.

hoop stresses (prestresses) at various locations within the ceramic. The stress measurements are through thickness averages, measured at two locations ($r = 0$ and 40 mm), and are used to evaluate the accuracy of the stress state produced from the computation.

The numerical technique used to produce ceramic prestress is performed in five distinct steps. The first step generates the target components (titanium confinement and ceramic), where the ceramic is slightly larger than the inside dimensions of the titanium confinement (the sliding/contact surfaces are not yet defined). The second step applies a pressure to the ceramic, compressing it to a size smaller than the confinement. The third step adds contact/sliding interfaces to the computation such that the ceramic surface and the confinement are recognized. The fourth step gradually removes the pressure on the ceramic. As the pressure is removed the ceramic increases in size until it comes in contact with the inner surface of the confinement material and a prestress is obtained. Because this process is done dynamically, stress oscillations in the target occur, requiring an important final step. In the final step a damping algorithm [6] is applied to eliminate the oscillations and bring the target to a steady state (at rest) condition. It is important to eliminate these stress oscillations because they can combine with stresses that occur from projectile impact, causing premature failure of the ceramic [7]. This approach to prestressing provides flexibility in determining the magnitude of the prestress. Changing the initial dimensions of the ceramic will change the magnitude of the prestress. It should be noted that this dynamic prestressing technique may produce slightly more plastic deformation in the confinement material than if done quasistatically (because the maximum dynamic response is greater than the final quasistatic response). It is expected that the differences will not be significant. It should also be noted that the material response for the metal is adiabatic which will produce a slightly softer response than if performed isothermally.

Fig. 1 shows the final stress state of the target, the damped response at the center of the target, and a comparison to experimentally measured stresses [3] in the target. The model and constants used for the AD99.5 alumina are from Anderson et al. [8]. The Johnson–Cook model was used for the confinement [9], and the titanium constants are from Meyers and Kleponis [10]. The diameter and thickness of the ceramic are $d_{cer} = 101.96$ mm and $t_{cer} = 12.745$ mm, respectively. The inner diameter and height of the confinement are $d_{con} = 101.60$ mm and $h_{con} = 12.700$ mm, respectively. The ceramic is larger than the confinement in both the radial ($\delta_r^* = d_{cer}/d_{con} = 1.0035$) and axial ($\delta_z^* = t_{cer}/h_{con} = 1.0035$) directions by the same proportion. This proportionality factor ($\delta_r^* = \delta_z^* = 1.0035$) was chosen to produce the same radial stress in the center of the target ($r = 0$) that was obtained experimentally (463 MPa). The overall stress state produced from the computation compares reasonably well with the stress state measured experimentally. One point of interest is the axial stress spike that occurs approximately every 100 μs after the prestress has been applied (shown in the stress–time history plot in Fig. 1b). These spikes are the result of the top and bottom titanium plate impacting the ceramic (oscillating), which occurs due to the dynamic prestress technique. The damping algorithm also reduces these axial stress spikes.

3. Computed results

Computed results for two target configurations are presented; a thin target, as previously discussed, and a thick target, as defined by Lundberg et al. [11]. The computations were

performed with 2D Lagrangian finite elements [12], meshless particles [13], the Johnson–Cook strength and fracture models for metals [9,14] and the JH-1 ceramic model [15]. The computations involve severe distortions, where the finite elements are automatically converted into meshless particles during the course of the computations [16]. The initial grid for the thin target uses seven crossed triangular elements (four triangles in a quad) across the radius of the projectile, and similar sizes elsewhere. The thick target uses a coarser mesh, where three crossed triangular elements across the radius of the projectile are used. The ceramic used for both targets is silicon carbide [17].

For both targets two prestress levels (small and large), and two prestress states (radial and hydrostatic) are investigated. The small prestress is similar in magnitude to values obtained experimentally [3,11]. The large prestress is approximately the maximum prestress the confinement can produce (determined computationally). The radial prestress is defined by $\delta_r^* > 1.00$ and $\delta_z^* = 1.00$. The hydrostatic prestress is defined by $\delta_r^* = \delta_z^* > 1.00$. It should be noted that the radial prestress is not purely radial because of Poisson's effect (which creates some axial stress) and the hydrostatic prestress is not purely hydrostatic because of the confinement deformation.

The ballistic performance for both the thin and thick target configuration is presented for the different prestress conditions. Penetration, perforation and dwell are used to evaluate the ballistic performance of the targets and to compare the effect of the various prestress conditions.

3.1. Thin target

Fig. 2 presents the results of a steel projectile impacting a thin ceramic target, with and without prestress. The steel projectile is modeled using the Johnson–Cook strength and fracture models for 4340 steel [9,14]. The target is identical to the one presented in Fig. 1 except the AD99.5 alumina ceramic core is replaced with silicon carbide. Silicon carbide is used because it has been well characterized for impact conditions [17]. For the prestressed target, the ceramic is oversized in both the radial and axial dimension ($\delta_r^* = \delta_z^* = 1.0035$) creating a small hydrostatic prestress (the same as was used in Fig. 1) and is presented in the top portion of Fig. 2. The pressure in the prestressed target is primarily in the range of 250–350 MPa and is relatively uniform. Damage contours are presented for both targets after projectile impact. At 15 μs after impact, both targets show that much of the ceramic has failed, although less has failed in the prestressed target. At 200 μs after impact both projectiles have exited the targets. The residual projectile exiting the prestressed target has less residual mass (M_r) and a lower residual velocity (V_r) than the projectile exiting the target without prestress. The pressure in the prestressed target, although relatively small, has a significant effect. The prestress produces a ceramic that is stronger, more ductile and less likely to fail in tension.

Fig. 3 presents four levels of hydrostatic prestress ($\delta_r^* = \delta_z^* = 1.0035$, 1.01, 1.02 and 1.03) used to determine the maximum prestress the confinement can produce. Fig. 3 presents both the pressure contours, and equivalent plastic strain contours, for the four cases. It is clear that the prestress is largest when $\delta_r^* = \delta_z^* = 1.01$. As $\delta_r^* = \delta_z^*$ increase above 1.01, the plastic strains in the titanium increase such that the peak confinement can no longer be maintained. The plastic strains are concentrated at the corners due to the "pinching" of the ceramic, causing the top and bottom cover plate to deform outward (away from the ceramic). The outward movement of the plates results in no axial stress in the center portion of the ceramic.

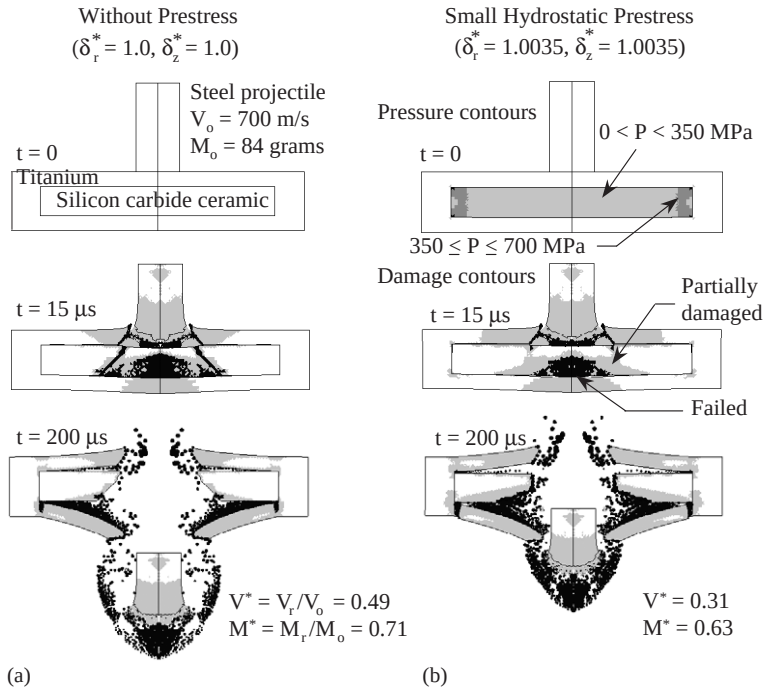

Fig. 2. Computed results for a steel projectile impacting (a) a thin target without prestress and (b) a thin target with a small hydrostatic prestress. The results show pressure contours at $t = 0$ and material damage at 15 and 200 μs after projectile impact.

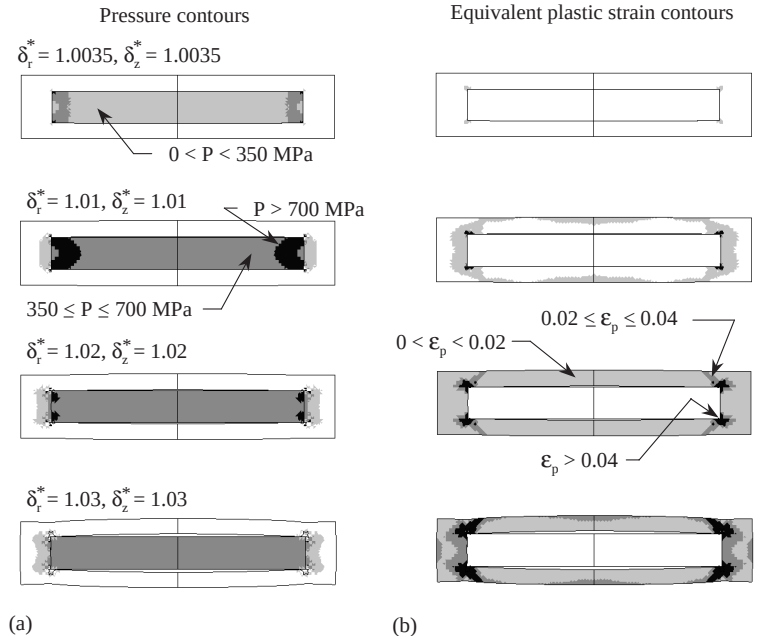

Fig. 3. Computed results for a thin axisymmetric target subjected to four levels of hydrostatic prestress. Shown are the (a) pressure contours and (b) equivalent plastic strain contours resulting from the prestresses.

Fig. 4 presents computed results for a steel projectile impacting a target without prestress, a target with a large radial prestress ($\delta_r^* = 1.01, \delta_z^* = 1.00$), and a target with a large hydrostatic prestress ($\delta_r^* = \delta_z^* = 1.01$), at an impact velocity of 700 m/s. The magnitude of the prestress was determined from Fig. 3. The pressures produced from the prestresses are shown on the top of Fig. 4. For both prestress conditions, the pressure is fairly uniform throughout the ceramic, although it is slightly greater at the edges due to the pinching from the confinement. Note that the pressure produced from the radial prestress is slightly larger (about 20 MPa) than that produced from the hydrostatic prestress. This is due to less plastic deformation in the radial prestress condition, which produces a larger radial and hoop stress. Damage contours are shown at various times after projectile impact. At 10 μs after impact it is clear that the target without prestress has the most failed ceramic, and a cone crack that runs through the thickness. Both prestressed targets

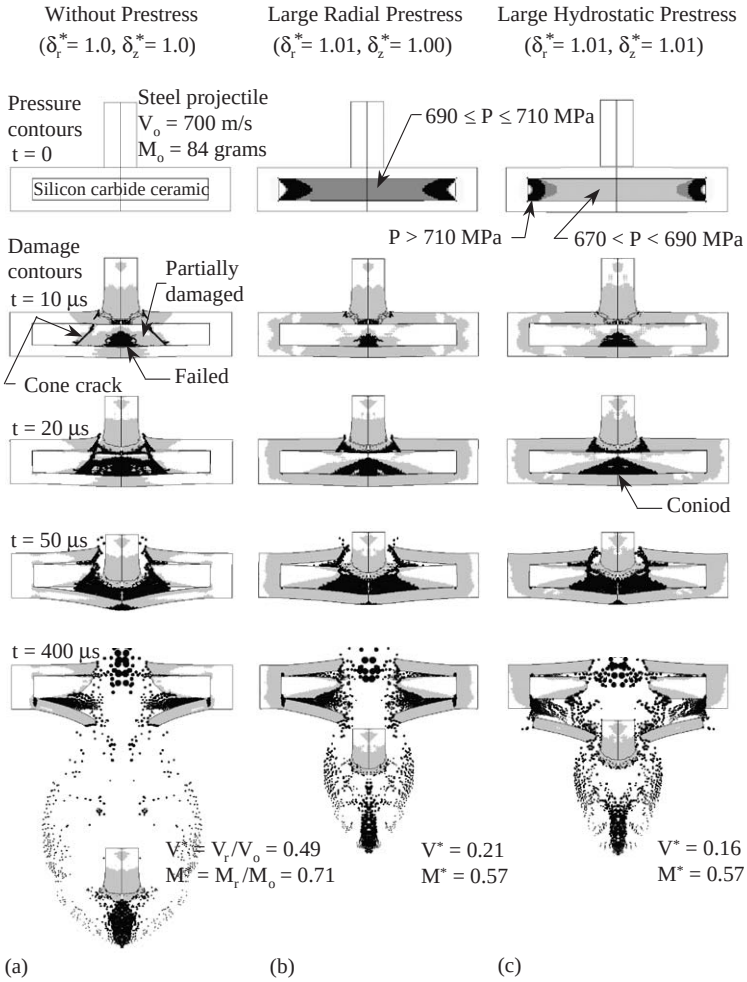

Fig. 4. Computed results for a steel projectile impacting (a) a thin target without prestress (b) a thin target with a large radial prestress and (c) a thin target with a large hydrostatic prestress. Also shown are pressure contours at $t = 0$ and damage contours at $t = 10$, 20, 50 and 400 μs after impact.

show much less damage than the target without prestress. The radial prestressed target shows the least amount of damage because of the higher initial pressure. At 20 μs the target without prestress shows that nearly all the ceramic directly under the projectile has failed. The prestressed targets exhibit much less failed ceramic. By 50 μs the ceramic under the projectile has failed for all three targets, although the target with no prestress shows the projectile much farther into the target. At 400 μs the projectiles are all exiting the targets. It is clear that the target with no prestress provides the least amount of resistance, with the projectile exiting with much greater velocity and mass. The results for the two prestressed targets are very similar except for the shearing of the back plate in the hydrostatic prestressed target. Back plate shearing occurs because of the larger initial plastic strains that result from the initial hydrostatic prestress. Another point of interest is the debris field located in front of the exiting projectiles. This debris field is primarily failed ceramic, and is concentrated on the axis of symmetry due to the "funneling" of the ceramic as it passes through the perforated back plate.

Fig. 5 shows the computed projectile kinetic energies, as a function of time, for the three targets presented in Fig. 4. The results from the radial and hydrostatic targets are nearly identical. The result for the target without prestress begins to deviate about 25 μs after impact, which is approximately when all the ceramic beneath the penetrator fails. Between 40 and 50 μs very little projectile energy is consumed for the target without prestress. The penetrator pushes the cone of failed ceramic into the back plate, which provides very little initial resistance. It should be noted that the projectile kinetic energies presented here are from the finite elements only and not the meshless particles. This gives projectile kinetic energies that are slightly lower than if the meshless particles were included, but the resulting trends should not change.

Prestressing enhances the ballistic performance of thin targets primarily because the dominant failure mode (tension) is delayed at the rear ceramic/metal interface. By delaying

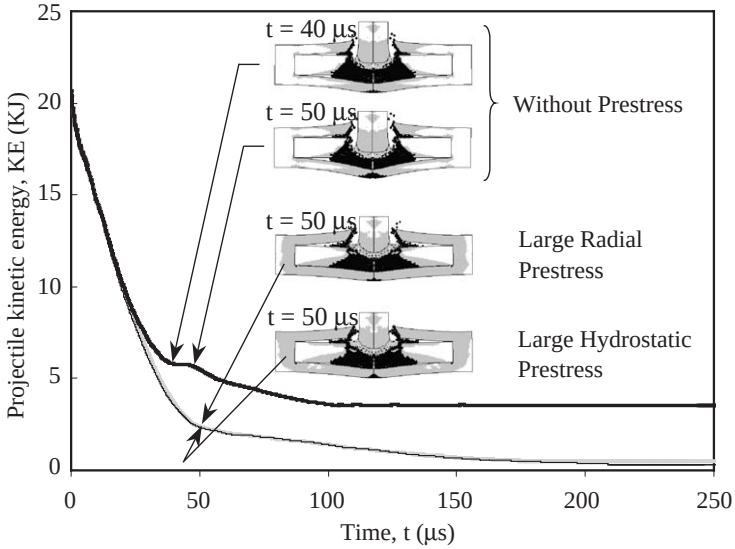

Fig. 5. Computed results showing projectile kinetic energy as a function of time during impact and penetration of a thin target with three levels of prestress. (Results are almost identical for the radial and hydrostatic prestress.) Also presented are damage contours at 50 μs after projectile impact for the three targets.

failure, the projectile interacts with intact ceramic for a longer time, resulting in increased target resistance.

3.2. Thick target

The thick target geometry is from Lundberg et al. [11] and is presented in Fig. 6. The projectile is a tungsten rod 80 mm in length and 2 mm in diameter. The target is silicon carbide confined by a high strength steel tube with a steel top and bottom plate. The confinement dimensions (inside) are 20 mm in diameter and 20 mm in height. The ceramic diameter, D, and height, H, are varied to produce the desired prestress. The ceramic model and silicon carbide constants are the same as those used for the thin target [15,17]. The Johnson–Cook strength and fracture model constants used for the tungsten projectile, high-strength steel tube and steel plugs were modified slightly from original published values [9,14,18] to more closely represent the materials used. The density, yield strength, hardening coefficient and bulk modulus of the tungsten were changed to 17,600 kg/m^3, 1.3, 0.18 and 285 GPa, respectively. The yield strength for the high-strength steel tube (S-7 tool steel) and steel plugs (4340 steel) were changed to 2.0 and 0.6 GPa, respectively.

Computed results for a small ceramic prestress (radial and hydrostatic), are presented in Figs. 7 and 8. The prestressed conditions are listed in Table 1 and are similar in magnitude to the experimental dimensions [11]. The three impact velocities are $V = 1410$, 1645 and 2175 m/s; and are identical to the ones used experimentally [11].

The upper portion of Fig. 7 shows the pressure profiles in the targets due to the prestress. It is clear that the hydrostatic condition produces the largest overall prestress. It is also clear that the pressure in the ceramic is not uniform. The non-uniform pressure occurs due to the non-uniform deformation of the confinement. Having a non-uniform pressure distribution in the ceramic can produce complex ballistic results; this will be discussed in more detail later when larger prestresses are used.

Results showing material damage are presented in the lower portions of Fig. 7, and the penetration into the ceramic as a function of time is presented in Fig. 8. At an impact velocity of

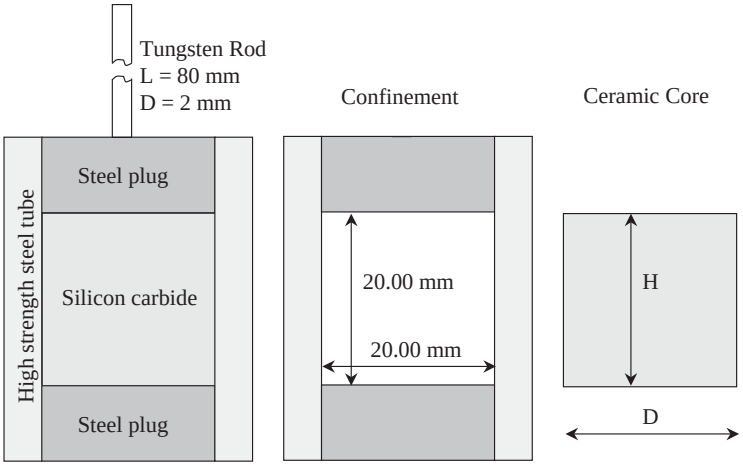

Fig. 6. Initial geometry of projectile, steel confinement and ceramic core for a thick target.

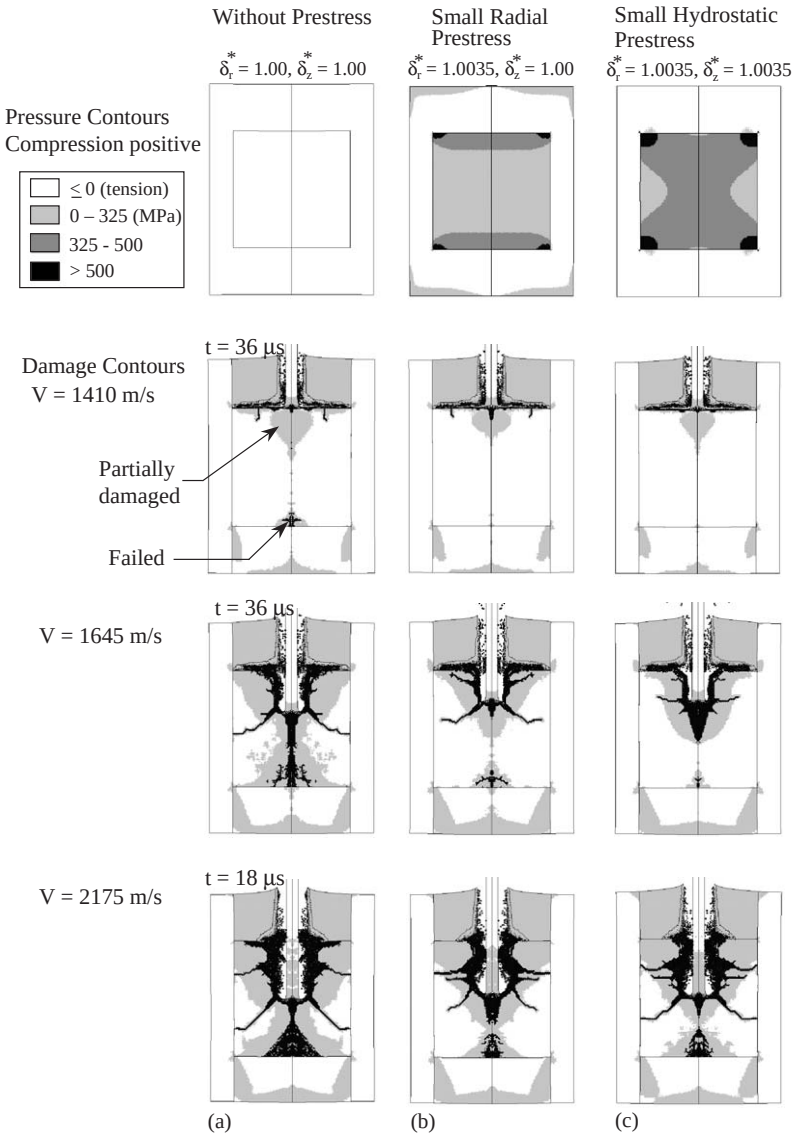

Fig. 7. Computed results for a tungsten projectile impacting a confined thick ceramic target. Three impact velocities and three target prestress conditions are presented. (a) Results for a target without prestress (b) with a small radial prestress and (c) with a small hydrostatic prestress.

1410 m/s there is no penetration into the ceramic for all three target conditions (sometimes referred to as ceramic dwell and/or interface defeat [7]). These results demonstrate that prestressing is not required to achieve interface defeat, although there is substantially more damage in the ceramic for the target without prestress, particularly at the rear ceramic/metal interface. There is little difference between the two prestressed targets. At an impact velocity of 1645 m/s the target with hydrostatic prestress exhibits the least amount of penetration (largest

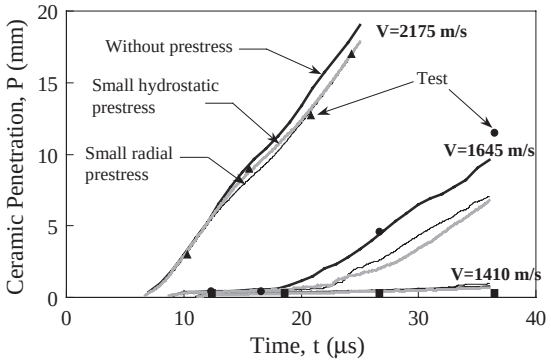

Fig. 8. Computed results showing penetration into the thick target ceramic, as a function of time, for three impact velocities and three target prestress conditions (with small prestresses).

Table 1
Dimensions of ceramic core for various thick target prestress conditions

Target prestress condition	D (mm)	H (mm)	$\delta_r^* = D/20$	$\delta_z^* = H/20$
Without prestress	20.00	20.00	1.00	1.00
Small radial prestress	20.07	20.00	1.0035	1.00
Small hydrostatic prestress	20.07	20.07	1.0035	1.0035
Large radial prestress	20.40	20.00	1.02	1.00
Large hydrostatic prestress	20.40	20.40	1.02	1.02

prestress pressure), the target with radial prestress has slightly more penetration (slightly less prestress pressure) and the target with no prestress produces the most penetration (no prestress pressure). The primary reason for the difference in penetration is due to the amount of ceramic dwell that occurs, but the rate of penetration also has a contributing effect. In Fig. 8 it is shown that at an impact velocity of 1645 m/s the targets with prestress dwell for about 4 μs longer than the target without prestress ($t = 18$ μs vs. $t = 22$ μs). The prestressed targets also exhibit a slightly reduced penetration rate. Both dwell and penetration rate are affected by pressure and the results presented in Fig. 8 are consistent with the initial prestress levels in the targets. The amount of damage in the targets (presented in Fig. 7) is also consistent with the magnitudes of the initial prestress. The hydrostatic prestress has the least amount of damaged ceramic (particularly at the rear ceramic interface), the radial prestress has slightly more, and the target without prestress exhibits the most. At an impact velocity of 2175 m/s the two targets with prestress produce essentially the same penetration while the target without prestress has slightly more penetration. The amount of damage that occurs at 18 μs after impact is again consistent with the amount of prestress. There is less difference in the results at the high velocity because the target is overmatched.

Fig. 9 presents four levels of hydrostatic prestress ($\delta_r^* = \delta_z^* = 1.0035$, 1.01, 1.02 and 1.03) used to determine the maximum prestress the confinement can produce. Fig. 9 shows both the pressure contours, and equivalent plastic strain contours, for the four cases. The largest prestress occurs

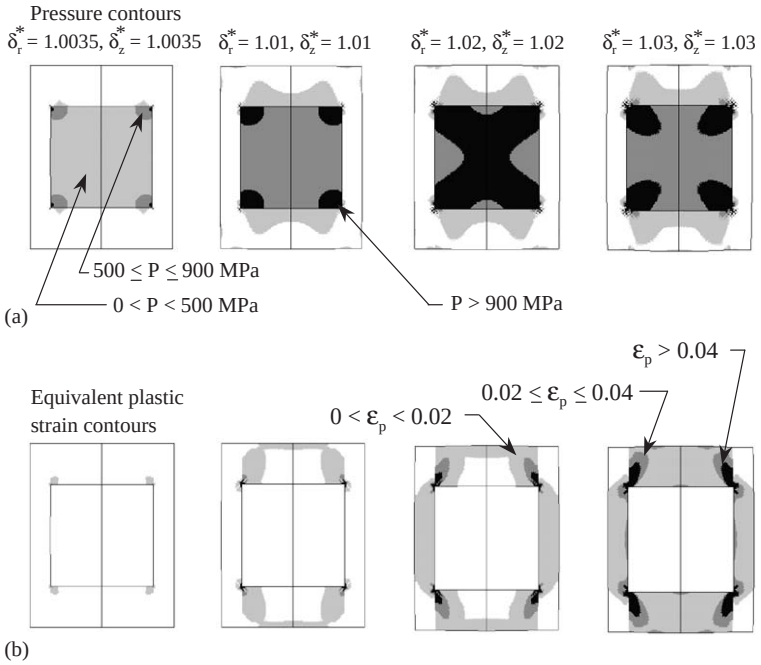

Fig. 9. Computed results for a thick axisymmetric target subjected to four levels of hydrostatic prestress. Shown are the (a) pressure contours and (b) equivalent plastic strain contours resulting from the prestresses.

when $\delta_r^* = \delta_z^* = 1.02$. As $\delta_r^* = \delta_z^*$ increase to 1.03, the plastic strains in the steel increase such that the peak confinement can no longer be maintained. The plastic strains are concentrated at the corners due to the "pinching" of the ceramic (similar to the thin target). It also appears that the top and bottom plate are susceptible to shear failure due to the high concentration of plastic strain along the tube/cover interface. The pressure profile produced from $\delta_r^* = \delta_z^* = 1.02$ has a unique shape due to the deformation of the confinement where the peak pressure contour occurs in an x-shaped pattern.

Figs. 10 and 11 present computed results for a tungsten projectile impacting a target without prestress, a target with a large radial prestress ($\delta_r^* = 1.02$, $\delta_z^* = 1.00$), and a target with a large hydrostatic prestress ($\delta_r^* = \delta_z^* = 1.02$). The prestressed conditions are listed in Table 1 and were determined to be the largest the confinement could produce (from Fig. 9). The three impact velocities are $V = 1410$, 1645 and 2175 m/s.

The upper portion of Fig. 10 shows the pressure profiles in the targets due to the prestress. As with the small prestress, the hydrostatic condition produces the largest overall prestress and again the pressure in the ceramic is not uniform. The non-uniform pressure occurs due to the non-uniform deformation of the confinement. Note that for the hydrostatic condition, along the axis-of-symmetry, the pressure is smaller at the surface of the ceramic than in the center, but for the radial prestress condition the pressure is greater at the surface and smaller in the center. This difference in pressure profiles occurs due to the difference in the initial ceramic geometry and the resulting deformation of the confinement material. The deformation in the confinement, produced from the hydrostatic condition, causes the top and bottom plate to deform away from the ceramic

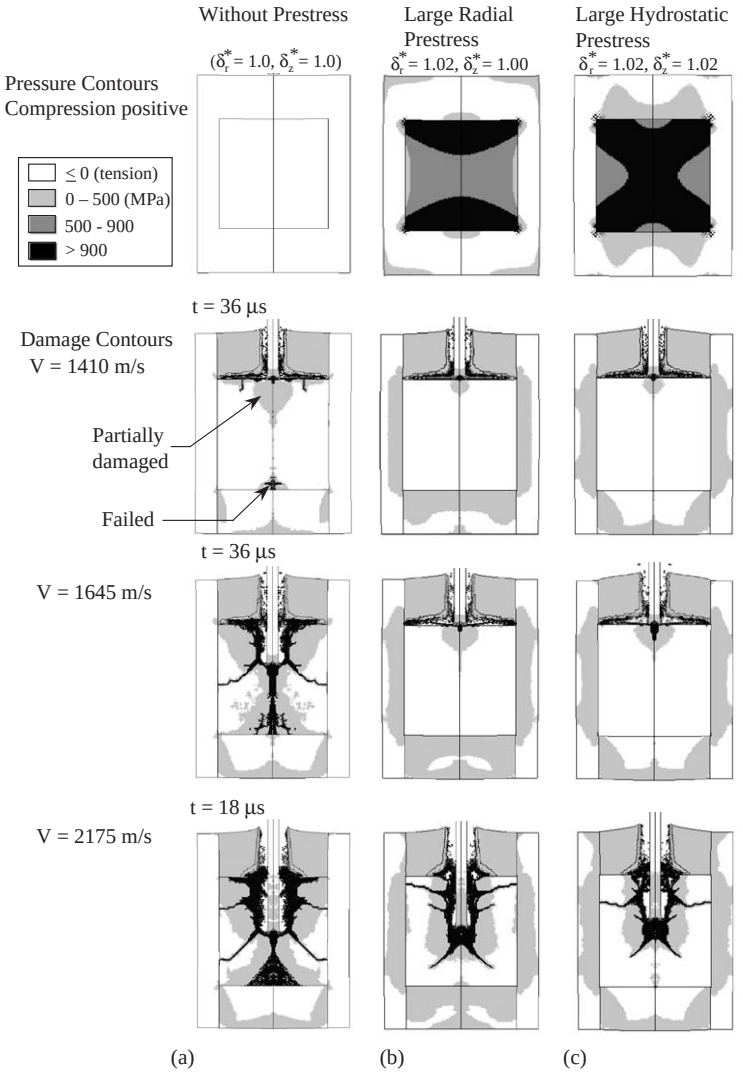

Fig. 10. Computed results for a tungsten projectile impacting a confined thick ceramic target. Three impact velocities and three target prestress conditions are presented. (a) Results for a target without prestress (b) with a large radial prestress and (c) with a large hydrostatic prestress.

(similar to the thin target), reducing the pressure at the surface. This same effect also occurs in the radial direction where the pressure on the surface is smaller than in the center. The large radial prestress condition has a similar effect in the radial direction (lower surface pressure), but because the ceramic is not oversized in the axial direction ($\delta_z^* = 1.00$) the pressure is more uniform on the top and bottom surface. The difference in pressure profiles, between the radial and hydrostatic prestress condition, has an important effect on the ballistic performance and will be discussed next.

The ballistic results for the two large prestress conditions (and the target without prestress included for comparison) are presented in Figs. 10 and 11. In the lower portions of Fig. 10, target

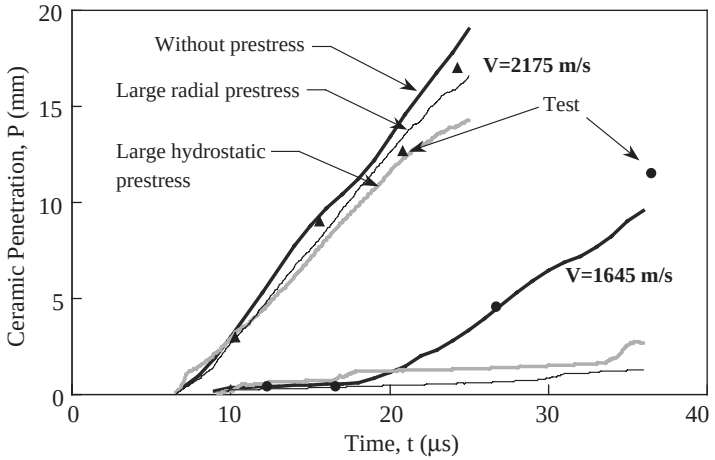

Fig. 11. Computed results showing penetration into the thick target ceramic, as a function of time, for two impact velocities and three target prestress conditions (with large prestresses).

damage is shown for the three target configurations and for the three impact velocities. Fig. 11 shows the penetration into the ceramic for the two highest impact velocities (1645 and 2175 m/s) against the three target prestress conditions. At an impact velocity of 1410 m/s there is no penetration into the ceramic. Both the large radial and large hydrostatic prestressed targets show very little damage (none at the rear ceramic surface) while the target without prestress shows substantial damage. At an impact velocity of 1645 m/s there is no penetration into the ceramic for the two prestressed targets. The large prestress has increased the ceramic dwell time to at least 36 μs. It also appears that there is more damage to the ceramic, in the target with the hydrostatic prestress, than with radial prestress. This occurs because the pressure at the ceramic surface is less for the hydrostatic prestress condition. At an impact velocity of 2175 m/s there is much more damage in the target without prestress, particularly at the rear interface. Another interesting observation is that the penetration rate is lower for the target with hydrostatic prestress than the target with radial prestress (see Fig. 11). The lower penetration rate occurs due to the higher prestress pressure in the interior of the hydrostatic prestressed target.

For the thick target, the results indicate that a large radial prestress condition provides improved ceramic dwell behavior because of the high surface pressure. The results also indicate that the large hydrostatic prestress condition provides more resistance during penetration because the interior pressure in the ceramic is higher. In either case, the results demonstrate that the ballistic performance of confined ceramic targets can be improved by prestressing the ceramic and that the prestressing phenomenon can be complex.

4. Summary

This article has presented computed results for the responses of ceramic targets, with and without prestress, subjected to projectile impact. A computational technique to include ceramic prestress was also presented. Thin and thick target configurations were used to understand the

effect of prestressing on ballistic performance. Two prestress levels (small and large) and two prestress states (radial and hydrostatic) were investigated. The results of this study are as follows:

- The ballistic performance of both target geometries (thin and thick) was improved by prestressing (independent of the type of prestress).
- Prestressing thin targets delays tensile failure at the rear ceramic/metal interface. By delaying ceramic failure, the projectile interacts with intact (stronger) ceramic for a longer time, resulting in improved ballistic performance.
- For thin targets there is little difference between the pressure produced from a hydrostatic prestress and a radial prestress, because the top and bottom plates are thin and have little rigidity.
- The magnitude of the prestress obtained from thick targets is greater than thin targets because the top and bottom plates are thicker and provide more confinement.
- The velocity at which ceramic penetration occurs (dwell-penetration transition velocity) can be increased in thick targets by prestressing.
- The penetration velocity into thick targets can be reduced by prestressing.
- The stress state that occurs from prestressing can be complex and needs to be understood to obtain the best possible ballistic improvement.

Acknowledgements

The authors would like to thank Dr. D.W. Templeton for his support in this work. The research reported in this document was performed in connection with Contract DAAD19-03-D-0001 with the US Army Research Laboratory. The views and conclusions contained in this document are those of the authors and should not be interpreted as presenting the official policies or positions, either expressed or implied, of the US Army Research Laboratory or the US Government unless so designated by other authorized documents. Citation of manufacturer's or trade names does not constitute an official endorsement or approval of the use thereof. The US Government is authorized to reproduce and distribute reprints for Government purposes notwithstanding any copyright notation hereon.

References

[1] Wilkins M, Honodel C, Sawle D. An approach to the study of light armor. UCRL-50284, Lawrence Livermore National Laboratory, June 1967.

[2] Weber K, El-Raheb M, Hohler V. Experimental investigation on the ballistic performance of layered AlN ceramic stacks. In: Reinecke WG, editor. Proceedings of the 18th International Symposium on Ballistics. San Antonio, TX: Technomic, 1999. p. 1247–54.

[3] Meyer Jr HW, Abeln T, Bingert S, Bruchey WJ, Brannon RM, Chhabildas LC, Dienes JK, Middleditch J. Crack behavior of ballistically impacted ceramic. In: Furnish MD, Chhabildas LC, Hixon RS, editors. Shock compression of condensed matter—1999, New York: AIP Press; 2000. p. 1109–12.

[4] Han C, Sun CT. A study of pre-stress effect on static and dynamic contact failure of brittle materials. Int J Impact Eng 2000;24(6–7):597–611.

[5] Holmquist TJ, Johnson GR. Modeling projectile impact onto prestressed ceramic targets. J Phys IV 2003;110: 597–602.
[6] Johnson GR, Beissel SR. Damping algorithms and effects for explicit dynamics computations. Int J Impact Eng 2001;25(9):911–25.
[7] Holmquist TJ, Johnson GR. A detailed computational analysis of interface defeat, dwell and penetration for a variety of ceramic targets. In: Carleone J, Orphal D, editors. Proceedings of the 20th International Symposium on Ballistics. Orlando, FL: DEStech; 2002. p. 746–53.
[8] Anderson Jr CE, Johnson GR, Holmquist TJ. Ballistic experiments and computations of confined 99.5% Al_2O_3 ceramic tiles. In: Mayseless M, Bodner SR, editors. Proceedings of the 15th International Symposium on Ballistics, vol. 2, Jerusalem, Israel; 1995. p. 65–72.
[9] Johnson GR, Cook WH. A constitutive model and data for metals subjected to large strains, high strain rates and high temperatures. Proceedings of the Seventh International Symposium on Ballistics. Netherlands: The Hague; 1983. p. 541–7.
[10] Meyer Jr. HW, Kleponis DS. Modeling the high strain rate behavior of titanium undergoing ballistic impact and penetration. Int J Impact Eng 2001;26(1–10):509–21.
[11] Lundberg P, Renstrom R, Lundberg B. Impact of metallic projectiles on ceramic targets: transition between interface defeat and penetration. Int J Impact Eng 2000;24(3):259–75.
[12] Johnson GR, Stryk RA, Holmquist TJ, Beissel SR. Numerical algorithms in a Lagrangian hydrocode. Report No. WL-TR-1997-7039, Wright Laboratory, June, 1997.
[13] Johnson GR, Beissel SR, Stryk RA. An improved generalized particle algorithm that includes boundaries and interfaces. Int J Numer Meth Eng 2002;53:875–904.
[14] Johnson GR, Cook WH. Fracture characteristics of three metals subjected to various strains, strain rates, temperatures and pressures. Eng Fracture Mech 1985;21(1):31–48.
[15] Johnson GR, Holmquist TJ. A computational constitutive model for brittle materials subjected to large strains, high strain rates and high pressures. Proceedings of EXPLOMET Conference. San Diego, CA, 1990.
[16] Johnson GR, Stryk RA, Beissel SR, Holmquist TJ. An algorithm to automatically convert distorted finite elements into meshless particles during dynamic deformation. Int J Impact Eng 2002;27(10):997–1013.
[17] Holmquist TJ, Johnson GR. Response of silicon carbide to high velocity impact. J Appl Phys 2002;91(9):5858–66.
[18] Holmquist TJ, Templeton DW, Bishnoi KD. Constitutive modeling of aluminum nitride for large strain, high-strain rate, and high-pressure applications. Int J Impact Eng 2001;25:211–31.